Waterborne Manganese Exposure Alters Plasma, Brain, and Liver Metabolites Accompanied by Changes in Stereotypic Behaviors

By: Steve Fordahl, Paula Cooney, Yunping Qiu, Guoxiang Xie, Wei Jia, and Keith M. Erikson

Fordahl, S., Cooney, P., Qiu, Y.P., Xie, G.X., Jia, W., Erikson, K.M. (2012). Waterborne manganese exposure alters plasma brain, and liver metabolites accompanied by changes in stereotypic behaviors. *Neurotoxicology and Teratology, 34*(1), 27-36.

Abstract:

Overexposure to waterborne manganese (Mn) is linked with cognitive impairment in children and neurochemical abnormalities in other experimental models. In order to characterize the threshold between Mn-exposure and altered neurochemistry, it is important to identify biomarkers that positively correspond with brain Mn-accumulation. The objective of this study was to identify Mn-induced alterations in plasma, liver, and brain metabolites using liquid/gas chromatography–time of flight–mass spectrometry metabolomic analyses; and to monitor corresponding Mn-induced behavior changes. Weanling Sprague–Dawley rats had access to deionized drinking water either Mn-free or containing 1 g Mn/L for 6 weeks. Behaviors were monitored during the sixth week for a continuous 24 h period while in a home cage environment using video surveillance. Mn-exposure significantly increased liver, plasma, and brain Mn concentrations compared to control, specifically targeting the globus pallidus (GP). Mn significantly altered 98 metabolites in the brain, liver, and plasma; notably shifting cholesterol and fatty acid metabolism in the brain (increased oleic and palmitic acid; 12.57 and 15.48 fold change (FC), respectively), and liver (increased oleic acid, 14.51 FC; decreased hydroxybutyric acid, − 14.29 FC). Additionally, Mn-altered plasma metabolites homogentisic acid, chenodeoxycholic acid, and aspartic acid correlated significantly with GP and striatal Mn. Total distance traveled was significantly increased and positively correlated with Mn-exposure, while nocturnal stereotypic and exploratory behaviors were reduced with Mn-exposure and performed largely during the light cycle compared to unexposed rats. These data provide putative biomarkers for Mn-neurotoxicity and suggest that Mn disrupts the circadian cycle in rats.

Article:

INTRODUCTION

Overexposure to environmental manganese (Mn) is known to have neurological consequences with symptomology similar to Parkinson's disease (PD) (Pal et al., 1999, Cersosimo and Koller, 2006 and Perl and Olanow, 2007). Both are characterized by alterations in the dopaminergic system of the basal ganglia, producing movement abnormalities and cognitive deficits (Pal et al., 1999 and Cersosimo and Koller, 2006). Mn neurotoxicity is clinically distinct from PD in that onset may occur at earlier ages, movement symptoms occur bilaterally as opposed to unilaterally

in PD, and the lack of response to levo-Dopa treatment (Cersosimo and Koller, 2006). Cases of Mn neurotoxicity have been reported due to occupational contact (e.g., mining, battery manufacturing, and welding) and contaminated drinking water (Crossgrove and Zheng, 2004 and Wasserman et al., 2006). Challenges exist in diagnosing Mn neurotoxicity, and factors such as length or route of exposure may differentially affect symptom onset. Inhalation of Mn species leads to rapid brain Mn accumulation and is associated with increased biomarkers of oxidative stress (Erikson et al., 2007); whereas, ingested Mn accumulates in the brain at slightly lower concentrations and is associated with neurochemical alterations (Garcia et al., 2006, Anderson et al., 2008 and Fordahl et al., 2010) and cognitive decline (Wasserman et al., 2006 and Bouchard et al., 2011).

Mn-neurotoxicity has been linked with changes in dopamine, γ-aminobutyric acid (GABA), and glutamate (Fitsanakis et al., 2006 for review). Mn-induced changes in these neurochemicals, specifically dopamine, have been associated with hyperactivity in rodents (Kern et al., 2010), and learning/memory deficits accompanied by changes in stereotypic behaviors in primates (Schneider et al., 2006 and Kern et al., 2010). Similar symptoms have been reported in Mn-exposed children (Bouchard et al., 2007 and Farias et al., 2010), and it is imperative to identify symptoms of toxicity early during this critical stage of growth and neurological development.

Early symptom identification and removal from Mn exposure can improve the prognosis of Mn neurotoxicity. The use of magnetic resonance imaging (MRI) has been demonstrated to accurately reflect brain Mn deposits (Dorman et al., 2006 and Fitsanakis et al., 2008), and when used in conjunction with positron emission tomography (PET) can identify biological alterations in neurotransmission (Kim et al., 1999). While MRI and PET technologies have advanced the identification of Mn neurotoxicity, the practical application and cost of these tools may preclude widespread use. Moving forward, it is important to establish cost effective diagnostic measures that correspond with brain Mn accumulation similar to MRI. Identifying biomarkers of Mn neurotoxicity in biological fluids may provide an alternative solution to confirm the extent of brain Mn accumulation.

To date, few reliable markers exist to measure the extent of brain Mn accumulation. Prospective compounds such as lymphocytic manganese superoxide dismutase (MnSOD) and arginase were suggested as biomarkers over a decade ago; however, each possessed diagnostic limitations (Davis and Greger, 1992 and Brock et al., 1994). More recently, Dorman et al. (2008) screened for potential Mn exposure biomarkers using a liquid chromatography–mass spectrometry method to identify metabolomic changes in the blood and urine of monkeys exposed to airborne $MnSO_4$. Of the 27 metabolites significantly altered by Mn, three blood metabolites corresponded with Mn accumulation in the globus pallidus (GP): phenylpyruvate, disaccharides, and guanosine (Dorman et al., 2008). While these markers show promise, additional studies are needed to confirm their potential as consistent biomarkers.

The study of metabolomics is emerging as a reliable approach to identify potential biomarkers in diseased states including cancer (Kim et al., 2008) and amyotrophic lateral sclerosis (Pradat and Dib, 2009), among other potential applications (Oresic et al., 2006). Methods using liquid and gas chromatography, coupled with mass spectrometry (LC–MS, GC–MS), enable the detection of thousands of metabolites in a biological sample (Halket et al., 2005). These methods are ideal

for monitoring changes in metabolite byproducts due to altered cellular metabolism in either a diseased state or after application of selected therapies. The goal of this study was to identify potential biomarkers of Mn neurotoxicity, and to link any changes in the metabolome with biological alterations associated with Mn-exposure. Additionally, we wanted to monitor any changes in behavior or locomotor activity indicative of neurotoxicity. While previous studies have examined the effects of Mn-exposure on behavior over short observational periods, to date no study has examined the effects of Mn on locomotor and circadian behaviors longitudinally over a 24 h period in a home-cage environment. A 24 h time frame allows for analysis of diurnal and nocturnal behaviors not normally captured with other behavioral tests.

MATERIALS AND METHODS

Animals

Male weanling (post-natal day 21) Sprague–Dawley rats (Harlan Sprague–Dawley, Indianapolis, IN) (n = 12) were individually housed and randomly divided into two treatment groups: control (AIN-93G diet (35, 10, and 6 mg/kg Fe, Mn, and Cu, respectively) with deionized water) and Mn-exposed (AIN-93G diet with deionized water containing 1 g Mn (as $MnCl_2$)/L). Formulated diet was obtained from Dyets Inc. (Bethlehem, PA). This Mn-exposure protocol has been used previously in our lab to achieve consistent brain Mn accumulation producing neurochemical changes indicative of toxicity after 6 weeks of exposure (Anderson et al., 2007, Anderson et al., 2008 and Fordahl et al., 2010). Based on average water consumption for rats (10–12 mL per 100 g body weight (Harkness and Wagner, 1989), Mn ingestion was approximately 100 mg/kg per day. Water levels were monitored to examine consumption, and no avoidance of Mn-containing water was observed. Because intestinal Mn absorption in rodents is estimated at 1–5% (Hurley and Keen, 1987), the systemic Mn burden was approximately 1–5 mg. Human exposure to waterborne Mn has been reported at > 700 μg/L in children (Wasserman et al., 2006) leading to cognitive impairment, and up to 14 mg/L in 25 Japanese adults (Kawamura et al., 1941) resulting in neurotoxicity (n = 23) and death (n = 2). Although 100 mg Mn/kg is considerably higher than documented human exposure, it should be noted that Sprague Dawley rats have a higher threshold for toxicity than humans withstanding Mn doses of 200 mg/kg/day for 2 yrs and 2251 mg/kg/day for 6 months before fatality (NTP, 1993 and Gianutsos and Murray, 1982). Rats had free access to food and water 24 h/day, with the lights off between 1800 and 600 h and room temperature maintained at 25 ± 1 °C. During the seventh week of the study, after an overnight fast with access to water, the rats were rendered unconscious in a CO_2 chamber, euthanized via decapitation, brains and liver tissue removed, and trunk blood was collected for analysis. Dissected tissues were immediately placed on dry ice then stored at − 80 °C until analysis. For metal analysis, sections of the globus pallidus (GP) and striatum, two regions known to accumulate Mn, were removed, and the remaining brain tissue was used for metabolomic analysis. The University of North Carolina at Greensboro Animal Care and Use Committee approved all of the animal procedures.

Hematology

Trunk blood from each rat was collected in heparinized tubes and stored on ice until processed. Hematocrit was determined by centrifugation of heparinized micro-hematocrit capillary tubes (Fisher Scientific, Waltham, MA). Remaining whole blood samples were centrifuged for 15 min at 1000 ×*g* to separate plasma for iron (Fe) status assays, metabolomic analysis and metal quantification. Plasma was stored at − 80 °C. Plasma ferritin and transferrin were determined

using enzyme linked immunosorbent assay (ELISA) kits from (ICL, Inc., Newberg, OR) and (GenWay Biotech, Inc., San Diego, CA), respectively.

Behavior analysis

Behavior analysis was conducted using Clever Systems Home Cage Scan (HCS) system (Reston, VA) rather than a rating scale system, which are generally time-consuming and provide ordinal data (Flagel and Robinson, 2007). The HCS system utilizes video images from the home cage acquired at 30 frames per second. Software algorithms then categorize the images into a set of behaviors by extracting the image of the animal movements. Based on the sequential postures of the animal and position of body parts in space, behaviors are assigned using pre-trained data sets as a reference (Flagel and Robinson, 2007). Agreement between behaviors identified by the HCS and manual assessments has been found to be ≥ 90% (Steele et al., 2007). During weeks four, five, and six of the dietary protocol, animals were placed in individual shoebox cages with food, water, and minimal bedding. The animals were allowed to acclimate to the novel environment for a 24 h period to ensure that any behavior alterations captured were treatment effects. After the acclimation period the animals were monitored by video surveillance and their behaviors were analyzed for an additional 24 h period to capture the entire light and dark cycle. Cameras were mounted onto tripods and placed parallel to the shoebox cages. Red lighting was utilized during the dark phase to provide an appropriate background for the HCS system to analyze movement. Behaviors were scored by the HCS system and data exported to MS Excel 2007 for analysis. The following behaviors were examined: total distance traveled, repetitive turning (turning), sniffing, rearing, and grooming.

Metal analyses

Mn, Fe, and copper (Cu) concentrations were measured with graphite furnace atomic absorption spectrometry (Varian AA240, Varian, Inc., USA). Brain, liver, and plasma samples were digested in ultra-pure nitric acid (1:10 dilution for plasma, 1:10 w/v dilution for tissue) for 48–72 h in a sand bath (60 °C). A 50 µL aliquot of digested sample was further diluted 1:20 with a 2% nitric acid solution for analysis. Bovine liver (NBS Standard Reference Material, USDC, Washington, DC) (10 µg Mn/g; 184 µg Fe/g; 80 µg Cu/g) was digested in ultrapure nitric acid and used as an internal standard for analysis (final concentration 5 µg Mn/L; 92 µg Fe/L; 40 µg Cu/L). Metal data are expressed as µg/g tissue or µg/L plasma. Additionally, an Fe:Mn ratio was also used to address the relationship between these metals as levels of one may impact the functionality or availability of the other (Chua and Morgan, 1996, Cowan et al., 2009 and Fitsanakis et al., 2008).

Liquid chromatography–time of flight mass spectrometry (LC–TOFMS)

Plasma samples were thawed and centrifuged at 13,000 rpm for 5 min. A volume of 100 µL supernatant was mixed with 400 µL of a mixture of methanol and acetonitrile (5:3). The mixture was vortexed for 2 min, allowed to stand for 10 min, centrifuged at 13,000 rpm for 20 min, and then the supernatant was used for LC–TOFMS. Liver and brain tissues (100 mg and 50 mg, respectively) were added to 500 µL of a chloroform, methanol, and water mixture (1:2:1, v/v/v). These samples were then homogenized and centrifuged at 13,000 rpm for 10 min at 4 °C. A 150 µL aliquot of supernatant was transferred to a sampling vial. The deposit was re-homogenized with 500 µL methanol followed by a second centrifugation. Another 150 µL

supernatant was added to the same vial for drying and then reconstituted in 500 μL of ACN:H_2O (6:4, v/v) before separation.

An Agilent HPLC 1200 system equipped with a binary solvent delivery manager and a sample manager (Agilent Corporation, Santa Clara, CA, USA) was used with chromatographic separations performed on a 4.6 × 150 mm 5 μm Agilent ZORBAX Eclipse XDB-C18 chromatography column. The LC elution conditions are optimized as follows: isocratic at 1% B (0–0.5 min), linear gradient from 1% to 20% B (0.5–9.0 min), 20–75% B (9.0–15.0 min), 75–100% B (15.0–18.0 min), isocratic at 100% B (18–19.5 min); linear gradient from 100% to 1% B (19.5–20.0 min) and isocratic at 1% B (20.0–25.0 min). For positive ion mode (ESI +) where A = water with 0.1% formic acid and B = acetonitrile with 0.1% formic acid, while A = water and B = acetonitrile for negative ion mode (ESI −). The column was maintained at 30 °C as a 5 μL aliquot of sample is injected. Mass spectrometry is performed using an Agilent model 6220 MSD TOF mass spectrometer equipped with a dual sprayer electrospray ionization source (Agilent Corporation, Santa Clara, CA, USA). The system was tuned for optimum sensitivity and resolution using an Agilent ESI-L low concentration tuning mix in both positive (ES +) and negative (ES −) electrospray ionization modes. Agilent API-TOF reference mass solution kit was used to obtain accurate mass time-of-flight data in both positive and negative mode operation. The TOF mass spectrometer was operated with the following optimized conditions: (1) ES + mode, capillary voltage 3500 V, nebulizer 45 psig, drying gas temperature 325 °C, drying gas flow 11 L/min, and (2) ES − mode, similar conditions as ES + mode except the capillary voltage was adjusted to 3000 V. The TOF mass spectrometer is calibrated routinely in ES + and ES − modes using the Agilent ESI-L low concentration tuning mix. During metabolite profiling experiments, both plot and centroid data are acquired for each sample from 50 to 1000 Da over a 25 min analysis time. Data generated from LC–TOFMS were centroided, deisotoped, and converted to mzData xml files using the MassHunter Qualitative Analysis Program (vB.03.01) (Agilent). Following conversion, xml files are analyzed using the open source XCMS package (v1.16.3) (http://metlin.scripps.edu), which runs in the statistical package R (v.2.9.2) (http://www.r-project.org), to pick, align, and quantify features (chromatographic events corresponding to specific m/z values and elution times). The software is used with default settings as described (http://metlin.scripps.edu) except for xset (bw = 5) and rector (plottype = “m”, family = “s”). The created .tsv file is opened using Excel software and saved as .xls file. The resulting 3-D matrix containing arbitrarily assigned peak index, retention time, and abundance value (.xls file) are further exported to SIMCA-P software 12.0 (Umetrics, Umeå, Sweden) for multivariate statistical analysis. Compound identification was performed by comparing the accurate mass and retention time with reference standards available in our laboratory, or comparing the accurate mass with online database such as the Human Metabolome Database (HMDB, 2011).

Gas chromatography–time of flight mass spectrometry (GC–TOFMS)

The GC–TOFMS analysis procedure was followed by our preious publications (Qiu et al., 2009 and Pan et al., 2010). For plasma sample (50 μL for each sample), the metabolites was extracted by 150 μL of mixture solvent (methanol:chloroform (3:1)). After centrifugation, an aliquot of the 170-μL supernatant was transferred to a glass sampling vial to vacuum dry at room temperature. The tissue samples were prepared identically to those used in the LC–TOFMS without reconstitution in ACN:H2O. Instead, the 150 μL alipuot of supernatant was added to the

same vial (containing 10 μL heptadecanoic acid in methanol, 1 mg/mL) to vacuum dry at room temperature. The residue of plasma and tissue samples was then derivatized by adding 80 μL methoxyamine (15 mg/mL in pyridine) to the vial while holding at 30 °C for 90 min, then 10 μL retention index compounds (the mixture of C10-C40, 50 μg/mL) and 80 μL BSTFA (1%TMCS) were added into the reaction vials. Then the samples were subjected to a 70 °C for 120 min derivatization reaction.

A 1 μL aliquot of the derivatized solution was injected using splitless mode into an Agilent 7890 N gas chromatograph coupled with a Pegasus HT time-of-flight mass spectrometer (Leco Corporation, St Joseph, USA). Separation was achieved on a DB-5 ms capillary column (30 m × 250 μm I.D., 0.25-μm film thickness; Agilent J&W Scientific, Folsom, CA, USA), with helium as the carrier gas at a constant flow rate of 1.0 mL/min. The temperature of injection, transfer interface, and ion source was set to 260 °C, 260 °C, and 210 °C, respectively. The GC temperature programming was set to 2 min isothermal heating at 80 °C, followed by 10 °C/min oven temperature ramps to 220 °C, 5 °C/min to 240 °C, and 25 °C/min to 290 °C, and a final 8 min maintenance at 290 °C. Electron impact ionization (70 eV) at full scan mode (m/z 40–600) was used, with an acquisition rate of 20 spectra/s in the TOFMS setting. The acquired MS files from GC/TOFMS analysis were exported in NetCDF format by ChromaTOF software (v4.22, Leco Co., CA, USA). CDF files were extracted using custom scripts (revised Matlab toolbox hierarchical multivariate curve resolution (H-MCR), developed by Par Jonsson, et al.) in the MATLAB 7.0 (The MathWorks, Inc, USA) for data pretreatment procedures such as baseline correction, de-noising, smoothing, alignment, time-window splitting, and multivariate curve resolution (based on multivariate curve resolution algorithm). The resulting three dimension data set includes sample information, peak retention time and peak intensities. Internal standards and any known artificial peaks, such as peaks caused by noise, column bleed and BSTFA derivatization procedure, were removed from the data set. The resulting data was mean centered and unit variance scaled during chemometric data analysis in the SIMCA-P 12.0 Software package (Umetrics, Umeå, Sweden). Compound identification was performed by comparing the mass fragments with NIST 05 Standard mass spectral databases in NIST MS search 2.0 (NIST, Gaithersburg, MD) software with a similarity of more than 70% and finally verified by available reference compounds.

Data analyses

Metal, body weight, hematology, and behavior data were analyzed using SPSS v14 for Windows. Data were examined for normality of distribution using a one-sample Kolmogorov–Smirnov test and for the presence of outliers by boxplot analysis. Independent *t*-test analyses were conducted to identify changes between control and Mn-exposed groups for metal, body weight, hematology, and behavior data. After Bonferroni correction for multiple comparisons, the significance level for metal and behavior *t*-tests was set at $p < 0.025$ and $p < 0.01$, respectively. Pearson's correlational analyses were then performed to examine relationships between metal concentrations, biomarkers, and behaviors, with a significance threshold set at $p < 0.05$.

Metabolomic LC/GC–TOFMS data was analyzed using principle component analysis (PCA) and OPLS analysis between groups. The differential metabolites were selected when they meet the requirements of variable importance in the projection (VIP) > 1 in OPLS model and $p < 0.05$

from student *t*-test. The corresponding fold change shows how these selected differential metabolites varied from control. Final data analysis between control and Mn-exposed groups for each metabolite was conducted using independent *t*-test analysis with a $p < 0.05$ significance threshold.

RESULTS

Body weight and hematology

Oral Mn-exposure alters systemic markers of iron status. Body weight measurements were completed three times per week to monitor growth. No significant change in body weight was observed between groups throughout the study, or in terminal body weight (Table 1). Because of the close relationship between biological Mn and Fe levels, we examined changes in hematological indicators of overall iron status due to Mn exposure. Mn-exposed rats had normal hematocrit levels but had significantly increased ($p = 0.016$) plasma transferrin accompanied by a trend toward reduced ferritin (Table 1) suggesting early stages of iron deficiency.

Table 1: Body weight and hematology.

Treatment	Body Wt. (g)	Hematocrit	Transferrin (mg/mL)	Ferritin (ng/mL)
Control	278.7 ± 6.3	0.50 ± 0.01	1.53 ± 0.06	425 ± 47.8
Manganese	263.3 ± 5.9	0.51 ± 0.01	2.21 ± 0.21*	299 ± 44.6

Values are listed ± SEM and significance was established using independent *t*-tests to identify differences between the control (n = 6) and Mn-exposed (n = 6) groups.
*($p \leq 0.05$).

Metal analyses

Oral Mn-exposure led to significantly elevated brain, liver, and plasma Mn concentrations. Mn, Fe, and Cu were quantified in dissected brain regions of Mn-exposed rats and non-exposed controls. Mn accumulated significantly in the striatum and GP ($p = 0.003$; $p = 0.019$, respectively) of Mn-exposed rats compared to controls (Table 2). Brain Fe levels were largely unaffected by Mn-exposure; however, due to Mn accumulation the Fe:Mn ratio was significantly lower in the striatum of Mn-exposed animals compared to controls (Table 2). While Fe homeostasis in the GP was quite stable under Mn exposure, Cu levels were significantly elevated ($p = 0.05$) due to Mn (Table 2). Although the Fe:Mn ratio was significantly lower in many brain regions, stable Fe levels suggest that metabolic and behavioral changes are driven by Mn accumulation, not Fe deficiency.

Table 2: Metal analysis of brain, liver, and plasma.

	Brain µg/g tissue			
	Mn	**Fe**	**Cu**	**Fe:Mn ratio**
Striatum				
Control	0.34 ± 0.06	6.1 ± 1.2	1.5 ± 0.2	21:1
Manganese	0.69 ± 0.06*	6.4 ± 1.3	1.5 ± 0.2	9:1*
Globus pallidus				
Control	0.57 ± 0.06	7.5 ± 1.8	0.9 ± 0.2	12:1
Manganese	1.03 ± 0.10*	9.5 ± 0.9	1.3 ± 0.1*	9:1
Liver µg/g tissue				
Control	2.31 ± 0.06	256 ± 31.1	4.3 ± 0.3	111:1
Manganese	5.10 ± 0.43*	92.6 ± 21.3*	4.4 ± 0.2	18:1**
Plasma µg/L				
Control	8.32 ± 0.35	1543 ± 112	838 ± 19	186:1
Manganese	26.5 ± 4.49*	1504 ± 256	848 ± 32	57:1*

Values are listed ± SEM and data were analyzed using independent *t*-tests to identify differences in metal content between the Mn (n = 6) and control (n = 6) groups.
*($p \leq 0.025$). **($p < 0.001$).

Similar to the brain, significantly higher Mn content was found in the liver of Mn-exposed rats compared to controls ($p = 0.002$) (Fig. 2). Elevated liver Mn was accompanied by dramatically reduced liver Fe levels ($p = 0.012$) and Fe:Mn ratio ($p < 0.001$) due to Mn-exposure. These data along with the transferrin and ferritin results indicate that Mn alters systemic Fe status leading to deficiency, without anemia. Liver Cu levels were comparable between Mn and control groups.

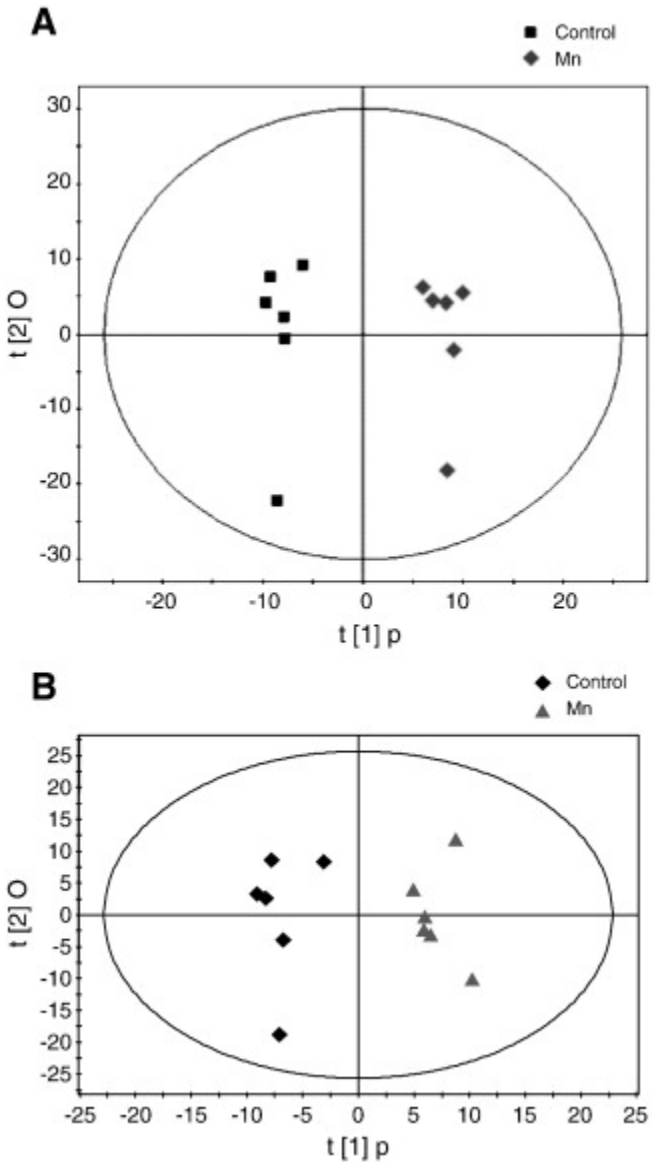

Figure 1: OPLS of plasma spectral data — A) Gas chromatography–time of flight–mass spectroscopy (GC–TOFMS) data represented by OPLS-DA scores plot between control and Mn-exposed groups. OPLS-DA Model: Control vs Mn, 1 + 2 components, R2X (cum) = 0.542, R2Xp = 0.152, R2Y (cum) = 0.977, Q2(cum) = 0.652. B) Liquid chromatography–time of flight mass spectroscopy (LC–TOFMS) data represented by the OPLS scores plot of the separation between healthy control and Mn-exposed rats. OPLS model: 2 component model, R2X = 0.395, R2Y = 0.934, Q2(cum) = 0.554.

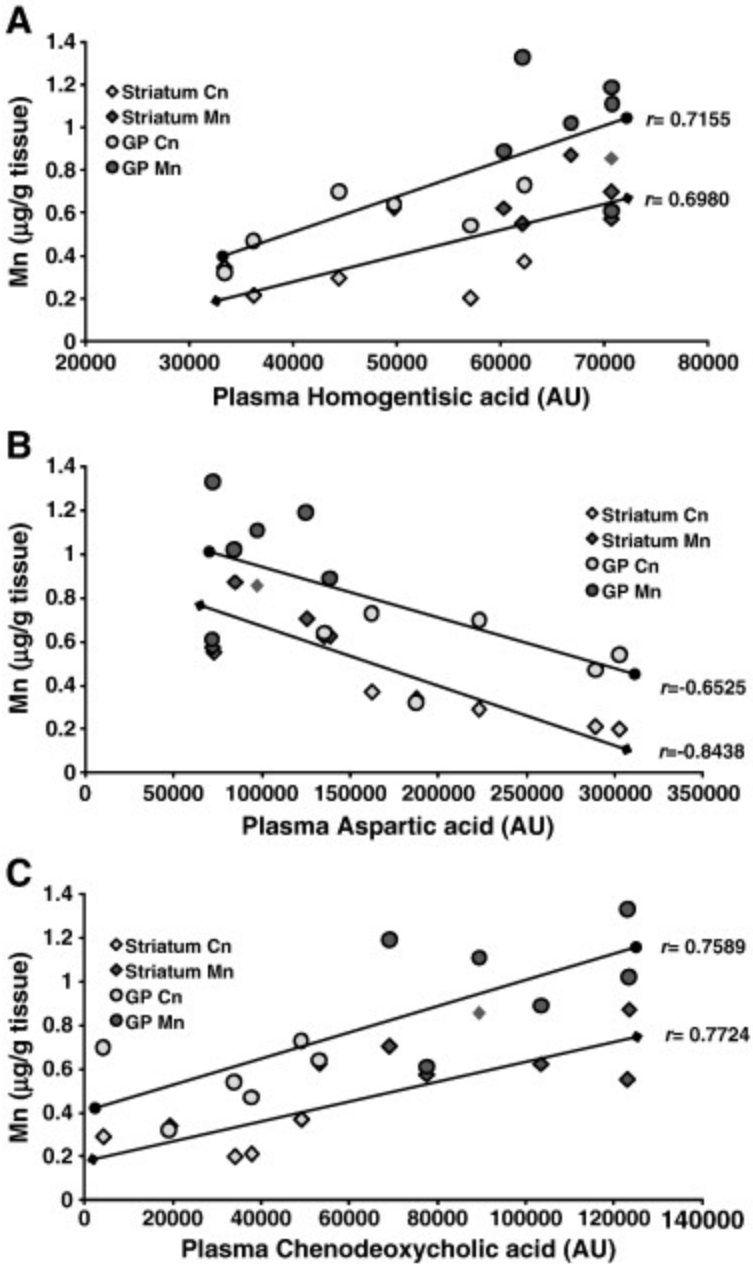

Figure 2: Relationships between brain Mn and plasma metabolites — Pearson's correlational analysis was conducted between plasma metabolites altered by Mn and Mn levels in the striatum and globus pallidus (GP). Significant relationships emerged between striatal and GP Mn levels with A) plasma homogentisic acid, B) aspartic acid, and C) chenodeoxycholic acid, represented by arbitrary units (AU), and depicted in scatterplot form with best fit trendlines representing the Pearson's *r* value for each plasma metabolite and brain region's metal content. Control (Cn) (n = 6) and Mn (n = 6) groups were included in the analysis and are depicted by shades of gray on each plot.

Plasma Mn concentrations were significantly increased in the Mn-exposed group versus control ($p = 0.013$). Plasma Fe and Cu levels were similar between groups, but the Fe:Mn ratio was significantly lower in Mn-exposed ($p = 0.003$), compared to control.

Metabolomic analyses

Mn-exposure significantly altered plasma, brain, and liver metabolites indicating a shift in the metabolome compared to controls. Metabolomic analysis of these tissues using LC/GC–TOFMS identified 98 significantly altered metabolites due to Mn-exposure. Significant changes were observed in each compartment: plasma (Table 3), brain (Table 4), and liver (Table 6), indicating changes in lipid and amino acid metabolism. Similarly, OPLS plots of plasma (Fig. 1), brain (Fig. 3), and liver (Fig. 4) data identify a shift in the metabolome of animals exposed to Mn versus healthy controls.

Table 3: Plasma metabolites altered with Mn-exposure.

Compound	FC	*p*
Cholesterol	1.35	0.008
2-Aminobutyric acid	1.24	0.043
2-Ethyl-3-hydroxypropionic acid	1.52	0.015
3,4-Dihydroxybutanoic acid	1.46	0.001
3-Hydroxybutyric acid	1.48	0.015
3-Indolepropionic acid	2.12	0.026
4-Hydroxy-proline	− 2.71	0.002
Alanine	− 2.00	0.041
Arginine	2.39	0.009
Aspartic acid	− 2.55	0.004
Chenodeoxycholic acid	2.98	0.000
Creatinine	− 2.50	0.009
Histidine	1.36	0.035
Homogentisic acid	2.39	0.009
Isocitric acid	1.76	0.002
Kynurenine	2.00	0.041
Methionine	1.21	0.027
Methyl phosphate	1.63	0.003
Myo-inositol, phosphate	1.52	0.005
Oxalic acid	1.29	0.043
Phenylalanine	1.34	0.017
Phosphate	1.83	0.014
Pseudo uridine	1.36	0.007
Uracil	1.31	0.023

Listed is the fold change (FC) of each metabolite in the Mn-exposed (n = 6) compared to control (n = 6) group, and its corresponding *p*-statistic. Independent *t*-tests were used to identify significance between Mn-exposed and control groups.

Table 4: Brain metabolites altered with Mn-exposure.

Compound	FC	*p*
2-Aminobutyric acid	1.28	0.010
2-Butenedioic acid	2.12	0.030
2-Pyrrolidone-5-carboxylic acid	− 2.79	0.029
3-Hydroxybutyric acid	1.46	0.005
4-Guanidinobutanoic acid	1.23	0.025
Acetyl aspartate	3.11	0.011
Arabitol	1.63	0.048
Ascorbic acid	1.60	0.004
Aspartic acid	− 1.10	0.024
Carnitine	− 1.10	0.011
Cholesterol	4.42	0.033
Citric acid	1.31	0.031
Desmosine	12.69	0.007
Fructose	1.41	0.028
Glycocholic acid	− 2.78	0.009
N-Acetyl-l-aspartic acid	1.55	0.004
Oleic acid	12.57	0.000

Palmitic acid	15.48	0.000
Phosphate	1.12	0.018
Proline	− 1.84	0.027
Sarcosine	1.33	0.006
Uracil	1.35	0.028
Urea	2.36	0.025
Valine	1.55	0.024

Listed is the fold change (FC) of each metabolite in the Mn-exposed (n = 6) compared to control (n = 6) group, and its corresponding *p*-statistic. Independent *t*-tests were used to identify significance between Mn-exposed and control groups.

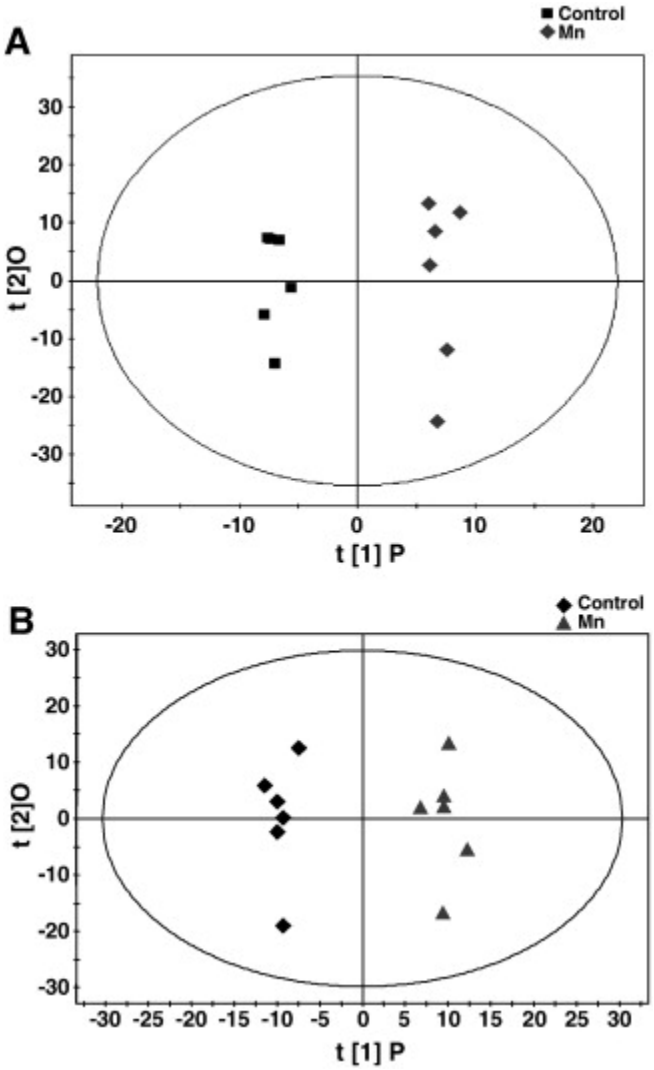

Figure 3: OPLS of brain spectral data — A) Gas chromatography–time of flight–mass spectroscopy (GC–TOFMS) data represented by OPLS-DA scores plot between control and Mn-exposed groups. OPLS-DA, Control vs Mn, 1 + 2 components, R2X (cum) = 0.462, R2Xp = 0.153, R2Y (cum) = 0.978, Q2(cum) = 0.526. B) Liquid chromatography–time of flight mass spectroscopy (LC–TOFMS) data represented by the OPLS scores plot of the separation between healthy control and Mn-exposed rats. OPLS model: 2 component model, R2X = 0.500, R2Y = 0.979, Q2(cum) = 0.642.

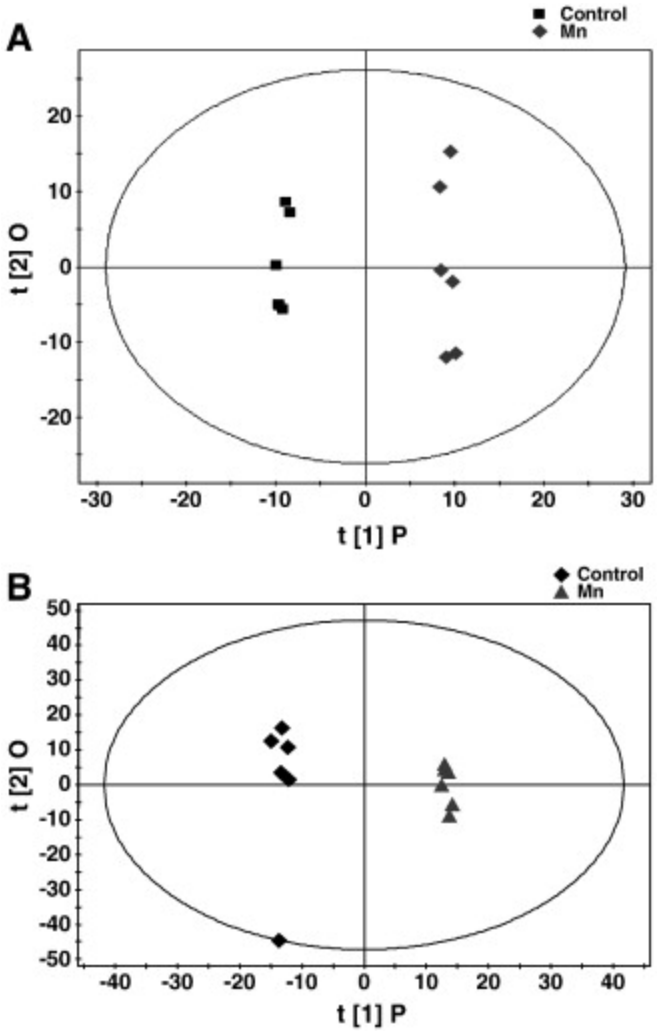

Figure 4: OPLS of liver spectral data – A) Gas chromatography–time of flight–mass spectroscopy (GC–TOFMS) data represented by OPLS-DA scores plot between control and Mn-exposed groups. OPLS-DA Model: Control vs Mn, 1 + 2 components, R2X (cum) = 0.454, R2Xp = 0.176, R2Y (cum) = 0.996, Q2(cum) = 0.695. B) Liquid chromatography–time of flight mass spectroscopy (LC–TOFMS) data represented by the OPLS scores plot of the separation between healthy control and Mn-exposed rats. OPLS model: 2 component model, R2X = 0.391, R2Y = 0.964, Q2(cum) = 0.660.

Several plasma metabolites altered by Mn reflect amino acid breakdown. Markers of tryptophan metabolism, 3-indolepropionic acid and kynurenine, were significantly elevated (2.12 fold change (FC); $p = 0.026$ and 2 FC; $p = 0.041$, respectively). Similarly, arginine and homogentisic acid levels were increased due to Mn, while alanine and creatinine were significantly decreased (Table 3). Significant associations were also identified between regional brain Mn accumulation and select plasma metabolites (Fig. 2). Positive correlations were found between plasma homogentisic acid and Mn levels in the striatum and GP ($r = 0.6980$, $p = 0.012$ and $r = 0.7155$, $p = 0.009$, respectively) (Fig. 2A), as well as substantia nigra Mn, GP Cu, and GP Fe levels ($r = 0.7068$, $p = 0.010$; $r = 0.6973$, $p = 0.012$; and $r = 0.6355$, $p = 0.026$, respectively) (data not shown). Similarly, chenodeoxycholic acid was positively correlated with striatal and GP Mn

($r = 0.7724$, $p = 0.003$ and $r = 0.7589$, $p = 0.004$, respectively) (Fig. 2C). These changes were accompanied by negative correlations between plasma aspartic acid and Mn in the striatum and GP (Fig. 2B). Additionally, correlations between metabolite changes and brain metals represent potential indices for brain metal homeostasis and Mn accumulation.

Mn altered brain metabolites indicative of compromised lipid metabolism and potential plasma membrane integrity including significant increases in cholesterol (4.42 FC; $p = 0.033$), desmosine (12.69 FC; $p = 0.007$), oleic acid (12.57 FC; $p < 0.001$), and palmitic acid (15.48 FC; $p < 0.001$) (Table 4). Changes in these lipids and several other brain metabolites were correlated with plasma Mn levels (Table 5). Alterations in oleic and palmitic acid may also suggest an impairment in fatty acid synthesis and energy metabolism, along with the significant increase in 2-butenedioic acid “Fumarate” (2.12 FC; $p = 0.030$). Mn caused a significant increase in urea (2.36 FC; $p = 0.025$) and decreased 2-pyrrolidone-5-carboxylic acid (− 2.79 FC; $p = 0.029$), which could be linked to disrupted glutamine metabolism.

Table 5: Brain metabolites correlated with plasma Mn.

Compound	*r*	*p*
2-Butenedioic acid	0.8415	< 0.001
Cholesterol	0.6208	0.031
Desmosine	0.8197	0.001
Glycocholic acid	− 0.6627	0.019
Oleic acid	0.8332	< 0.001
Palmitic acid	0.7589	0.004

Relationships between plasma Mn and altered brain metabolites were identified using Pearson's correlational analysis. *r* and *p* values are displayed for each metabolite significantly ($p < 0.05$) correlated with plasma Mn.

The largest effect Mn exposure had on liver metabolites pertained to lipid metabolism and ketone body formation; oleic acid (14.51 FC; $p = 0.003$) and hydroxybutyric acid (− 14.29 FC; $p = 0.048$), respectively (Table 6). Mn also significantly decreased metabolites associated with energy metabolism including creatine (− 3.13 FC; $p = 0.008$) and nicotinamide ribotide (− 3.03 FC; $p = 0.031$), and structural markers hydroxyglutaric acid, desmosine, and serine (6.47 FC, 5.25 FC, and 3.78 FC, respectively; $p < 0.002$) (Table 6). It is important to note that the liver metabolites altered by Mn-exposure were correlated with increased liver Mn concentrations and not decreased Fe levels (data not shown).

Table 6: Liver metabolites altered with Mn-exposure.

Compound	FC	*p*
1,4-Diaminobutane	1.40	0.022
1-Methyladenosine	1.37	0.001
2-Aminobutyric acid	1.34	0.033
3-Hydroxy-n-valeric acid	1.52	0.015
Aminocaproic acid	1.15	0.013
Aspartic acid	1.11	0.047
But-2-enoic acid	1.24	0.000
Cadaverine	1.93	0.008
Choline	− 1.19	0.041
Citicoline	1.59	0.007
Creatine	− 3.13	0.008
Cytidine	1.24	0.030
Desmosine	5.25	0.002
Dihydrothymine	− 3.03	0.012
d-Xylose-1-phosphate	− 1.48	0.010
Ethylmalonic acid	2.30	0.040
Glycerolphosphate	− 1.56	0.002
Homocitrulline	1.63	0.006
Hydroxybutyric acid	− 14.29	0.048
Hydroxyglutaric acid	6.47	0.001
Isoleucine	2.62	0.030
l-Cysteine	1.42	0.000
l-Methionine	1.15	0.044
Malonic acid	− 1.32	0.014
N,N-Dimethylglycine	1.47	0.038
N-Acetyl glucosamine	1.22	0.042
Nicotinamide ribotide	− 3.03	0.031
Norepinephrine	1.95	0.011
Norleucine	1.28	0.045
Octadecanedioic acid	1.58	0.013
Oleamide	1.57	0.040
Oleic acid	14.51	0.003
Pantothenic acid	1.25	0.007
Proline	1.55	0.006
Pyridoxamine	1.20	0.013
Pyroglutamic acid	− 1.13	0.045
Ribitol	1.67	0.050
Ribonic acid-1,4-lactone	2.19	0.000
Sebacic acid	1.15	0.018
Serine	3.78	0.001
Serotonin	1.27	0.034
S-Nitrosoglutathione	1.64	0.015
Stearic acid	− 3.33	0.017
Taurocholic acid	1.38	0.017
Threonine	1.19	0.022
Uracil	1.41	0.029
Urobilin	− 1.75	0.020
Valeric acid	1.22	0.050
Valine	1.17	0.048
Xanthosine	1.53	0.002

Listed is the fold change (FC) of each metabolite in the Mn-exposed (n = 6) compared to control (n = 6) group, and its corresponding *p*-statistic. Independent *t*-tests were used to identify significance between Mn-exposed and control groups.

Behavioral observations

Mn-exposure significantly increased locomotion and altered stereotypic activity associated with light and dark cycles. Because hyperactivity and altered locomotion has been previously associated with Mn-exposure ([Bouchard et al., 2007] and [Kern et al., 2010]) we conducted behavioral analysis during the fourth, fifth, and sixth weeks of Mn-exposure using 24 h video surveillance to monitor Mn-induced changes in activity. No changes in behavior occurred until the sixth week of exposure when total activity, measured as total distance traveled (TDT), was significantly greater ($p = 0.003$) in the Mn-exposed group (Fig. 5A); moreover, increased

locomotion was strongly correlated with GP, striatal, and plasma Mn levels ($r = 0.8027$, $p = 0.002$; $r = 0.7212$, $p = 0.008$; and $r = 0.6229$, $p = 0.030$, respectively) (Fig. 5A1, A2, and A3). Analysis of individual behaviors identified a significant increase in repetitive turning ($p = 0.007$) during the light cycle of Mn-exposed animals and a significant Mn-induced decrease in rearing ($p = 0.006$) during the dark cycle (Fig. 5B). Depicting behaviors as percent performed in the light cycle versus dark cycle revealed increased activity of Mn-exposed animals in the light cycle, contradictory to the nocturnal activity of the controls (Fig. 5C).

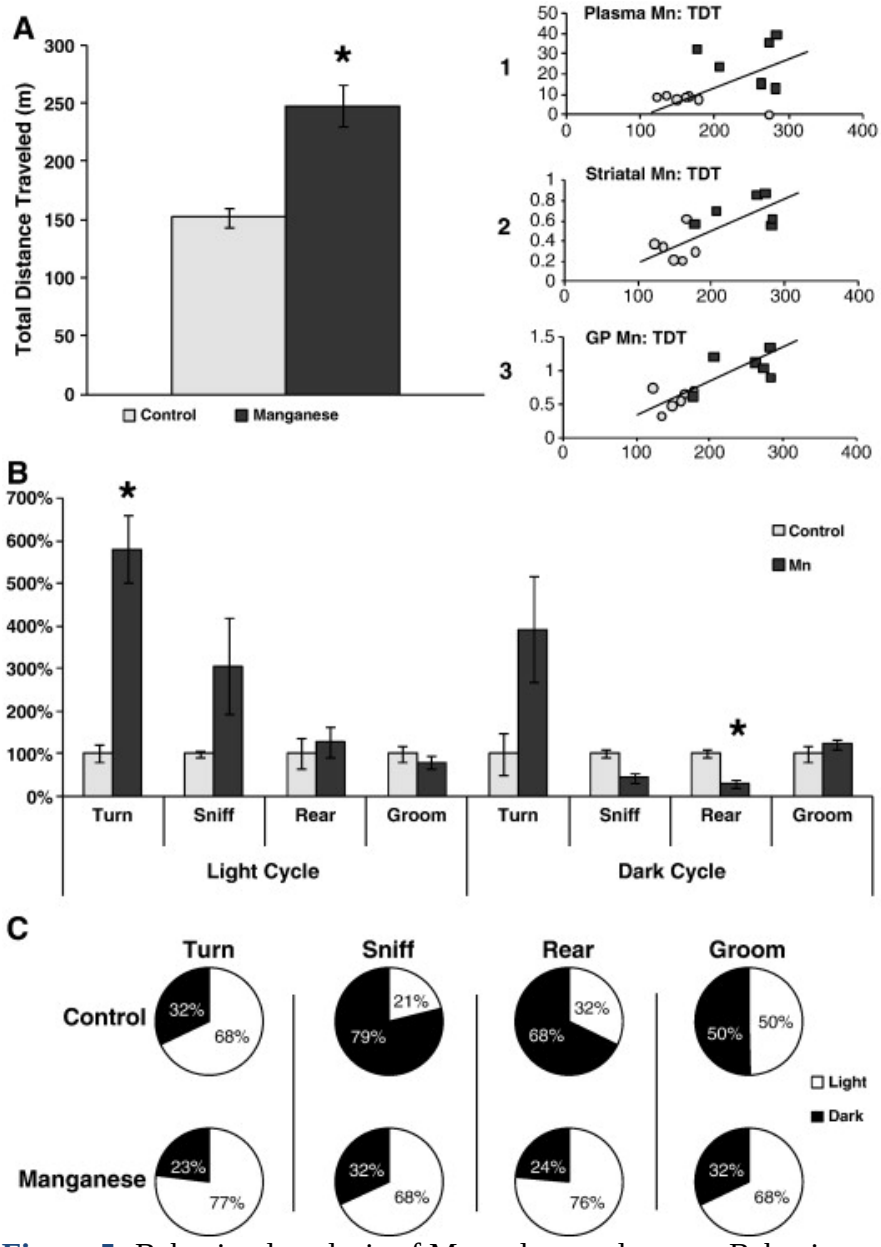

Figure 5: Behavioral analysis of Mn and control rats — Behaviors were monitored for 24 h using Home Cage Scan video surveillance during the sixth week of Mn-exposure. A) Total distance traveled (TDT) in meters over the 24 h period for control and Mn-exposed rats. Independent *t*-tests were used to identify differences between groups and data are

expressed ± SEM. Inset) Scatter plot representation of Pearson's correlational analysis between TDT (in meters; x axis) and 1) plasma Mn (μg/L; y axis) (r = 0.6229), 2) striatal Mn (μg/g; y axis) (r = 0.7212), and 3) globus pallidus (GP) Mn (μg/g; y axis) (r = 0.8027). B) Total behaviors expressed as percent control during the light and dark cycles using independent *t*-tests to identify differences between groups data are expressed ± SEM. (* = $p < 0.01$) C) Percentage of each behavior completed in the light or dark cycle for control and Mn-exposed rats.

DISCUSSION

The purpose of this study was to identify biomarkers of Mn-toxicity that provide diagnostic information corresponding to brain Mn accumulation, and to monitor changes in rat home cage behaviors that accompany Mn-accumulation. Using a LC/GC–TOFMS method of metabolomic analysis we were able to identify several potential biomarkers that corresponded with indices of Mn-neurotoxicity in rats; including, altered metal homeostasis, amino acid metabolism, and markers of structural damage. Additionally, video surveillance identified altered behavior and activity consistent with previous observations in Mn-exposure models; however, our 24 h data collection period identified a previously unreported disturbance in circadian rhythm due to Mn-toxicity.

Oral Mn-exposure elevated brain Mn in all regions examined, primarily localizing in the GP. A novel increase in Cu was also observed in the GP, but it is unclear whether the elevation in Cu is a direct effect or an artifact of Mn-exposure. For example, Mn can influence Fe homeostasis, evidenced by a decrease in the Fe:Mn ratio, which has been linked with elevated GP copper (Erikson et al., 2004). Similarly, liver and plasma Mn levels were increased with Mn-exposure. While Mn-exposure did not drastically alter brain or plasma Fe levels, it did significantly lower liver Fe content. Decreased liver Fe was accompanied by decreased plasma ferritin and increased plasma transferrin indicating systemic Fe deficiency but not anemia (normal hematocrit) (Table 1 and Table 2). It is important to note that while systemic Fe status was significantly altered due to Mn exposure, the metabolic and behavior alterations that occurred were strongly associated with increased brain Mn content and not depleted systemic iron.

Locomotor activity (i.e. total distance traveled) is often used in neuroscience as an outcome measure for neurotoxic effects (O'Donoghue, 1996 and Flagel and Robinson, 2007). In our study, increased overall activity, measured by TDT, was observed with Mn exposure, and was associated with plasma, striatal, and GP Mn levels (Fig. 5A). Increases in the motor activity of rats as a result of Mn exposure have been reported previously (Calabresi et al., 2001 and Kern et al., 2010), though these effects are often transient (Vacher et al., 2006). Repetitive turning was also observed in Mn-exposed rats, which may contribute to the overall increased activity, but has also been associated with stereotypy linked to dopaminergic dysfunction, akin to obsessive compulsive disorders (de Haas et al., 2010). While repetitive turning was significantly elevated in Mn-exposed rats the distribution of repetitive turning events was consistent with the circadian behavior of control animals, unlike rearing, sniffing and grooming (Fig. 5C). Rearing and sniffing behaviors were markedly decreased during the dark cycle of Mn-exposed rats, consistent with previous reports (Witholt et al., 2000). Changes in these exploratory behaviors contradict typical nocturnal behavior (Scheer et al., 2003) and suggest that Mn-exposure may disrupt the circadian clock. Sleep disturbances are common among Parkinson's disease patients (Suzuki et

al., 2011), and reversal of the circadian rhythm has been observed in iron deficient rats and is attributed to alterations in dopaminergic and/or noradrenergic activity (Youdim et al., 1980). In addition to dopamine and norepinephrine, circadian rhythm is largely influenced by serotonin, GABA, and glutamate in the suprachiasmatic nucleus (Wagner et al., 2001 and Reghunandanan and Reghunandanan, 2006), and circadian fluctuations in dopamine, glutamate, and GABA have been reported in the striatum of rats (Castaneda et al., 2004). Therefore, if the altered light/dark behaviors observed in this study are indeed alterations in circadian rhythm, they are likely driven by alterations in striatal dopamine, GABA and/or glutamate that have been linked with Mn-exposure (Fitsanakis et al., 2006 for review). Further studies utilizing larger sample size with longer monitoring periods are needed to confirm Mn-induced circadian reversal; however, these data suggest that Mn disrupts normal behaviors throughout the light/dark cycle as opposed to previously reported short observational periods (Youdim and Yehuda, 1985). While behavior is a valuable indicator of neurobiological function when assessing neurotoxicity; biochemical measures (e.g. metabolomics) are equally important to identify metabolic changes congruent with neurotoxicity, and to reveal potential biomarkers.

To our knowledge, the only other metabolomic analysis of Mn-exposure was completed by Dorman et al. (2008) in monkeys exposed to airborne $MnSO_4$. While the Mn exposure protocol between the two studies differed, there were similarities in altered blood metabolites, specifically elevated arginine and glutamine derivatives. Our study corroborated these previous data and revealed a few new scenarios. Possibly the most compelling identified a substantial impact of Mn on fatty acid metabolism in the brain. Palmitic acid, the product of *de novo* lipogenesis, was detected in 15-fold greater concentrations in the brains of Mn-exposed rats. Increased palmitate was accompanied by significant elevations in oleic acid, desmosine, and cholesterol (Table 4). Other than oleic acid, Mn did not have the same affect on these metabolites in the liver, which is interesting because Mn has been shown to increase lipogenesis in liver tissue despite high lipid availability (Baquer et al., 1974), possibly by inhibiting normal feedback mechanisms. Mn has also been linked to increased acetyl-CoA carboxylase activity, enhancing fatty acid synthesis (Scorpio and Masoro, 1970). Mn-enhanced lipogenesis could account for the increased palmitic acid (found in the brain) and its potential downstream product oleic acid (increased in brain and liver). Alternatively, Mn has been implicated in endoplasmic reticular stress (Chun et al., 2001 and Tjalkens et al., 2006), which may disrupt fatty acid elongation resulting in abnormally high palmitic acid content. Mn accumulation may also compromise liver function leading to liver damage or failure. Mn-induced liver failure will directly affect liver metabolites and may influence metabolite changes in other tissues including clearance and/or degradation.

Increased palmitic acid in the brain, along with elevated cholesterol, may introduce a scenario similar to what has been observed in Alzheimer's disease (AD). Palmitic acid has been linked to increase ceramide production in astrocytes (Patil et al., 2007) and implicated in the elevation of β-secretase (BACE1) activity and tau hyperphosphorylation (Patil et al., 2008). Additionally, elevated free cholesterol influences β- and γ-secretase activity enhancing amyloid β production (Shobab et al., 2005). Mn has also been directly linked to tau hyperphosphorylation in PC12 cells (Cai et al., 2011). Changes in lipid availability may also compromise membrane integrity by increasing fatty acid and cholesterol incorporation, thereby altering normal structure and dynamics. Continuity of vascular structure may also be compromised as elevated levels of

desmosine, a marker of elastin breakdown (Ronchetti and Contri, 1997), were found in the Mn-exposed group compared to control.

Evidence of compromised integrity existed in the brains of Mn-exposed rats. We speculate, however, that markers of structural damage were not linked to neuronal death. Neuronal loss due to structural damage has been associated with decreased *N*-acetylaspartate (NAA) levels (Demougeot et al., 2001), and a previous study on Mn-exposed primates observed decreases in NAA and the NAA:creatine ratio suggesting neuronal integrity/density was altered (Guilarte et al., 2006). We observed minimal changes in brain creatine levels and increased NAA due to Mn-exposure, and when coupled with altered lipid metabolites likely signify altered membrane integrity rather than neuronal death.

To investigate potential biomarkers associated with Mn-induced neurological dysfunction, we conducted correlational analyses between the plasma metabolites prominently altered by Mn with brain Mn concentrations in the striatum and GP. Notable plasma metabolites that were altered due to Mn were aromatic amino acids derivatives (Tryptophan: 3-indolepropionic acid and kynurenine; Tyrosine: homogentisic acid) (Table 3). Plasma homogentisic acid, aspartic acid, and chenodeoxycholic acid all correlated significantly with GP and striatal Mn accumulation (Fig. 2). Increased chenodeoxycholic acid is consistent with altered bile acid regulation in the liver (Table 6). Because plasma Mn correlated significantly with GP Mn we also examined relationships between plasma Mn and altered brain and liver metabolites. Weak correlations were found between plasma Mn and liver metabolites associated with energy production (e.g. creatine and ribonic acid) (data not shown); however, plasma Mn was a better predictor of altered lipid metabolism (cholesterol, palmitate and oleate) and structural integrity (desmosine) in the brain. In this aspect, plasma Mn may be useful to monitor along with plasma metabolites (e.g., chenodeoxycholic acid or homogentisic acid) in order to gain a more complete picture of brain Mn accumulation and its resulting pathologies possibly leading to earlier intervention.

In conclusion, 6 weeks of oral Mn-exposure led to increased brain Mn that corresponded with locomotor and stereotypic behavior abnormalities suggesting a disturbance in circadian rhythm. Simultaneous changes in brain, plasma, and liver metabolites were also identified and associated with brain Mn accumulation. Together, these data provide a useful starting point to identify metabolite biomarkers that correspond with Mn toxicity in a more cost effective manner. Furthermore, it may be prudent to consider how shifts in multiple metabolites may relate to one another in Mn-toxicity; for example, an indicator of brain Mn accumulation (plasma chenodeoxycholic acid predicts GP Mn) together with an indicator of Mn-induced changes in the brain (plasma Mn predicts elevated brain desmosine) will better appraise the progression of neurotoxicity. GC/LC–TOFMS can be a powerful tool to identify potential biomarkers, and additional study paradigms (route of exposure and/or species) are warranted to identify consistent biomarkers using this technique.

ABBREVIATIONS

Mn, manganese; PD, Parkinson's disease; GABA, γ-aminobutyric acid; MRI, magnetic resonance imaging; PET, positron emission tomography; MnSOD, manganese superoxide

dismutase; GP, globus pallidus; LC–TOFMS, liquid chromatography–time of flight mass spectrometry; GC–TOFMS, gas chromatography–time of flight mass spectrometry; Fe, iron; ELISA, enzyme linked immunosorbent assay; HCS, Home Cage Scan; Cu, copper; FC, fold change; TDT, total distance traveled; AD, Alzheimer's disease; Cn, control; NAA, *N*-acetylaspartate; HMDB, Human Metabolome Database

FUNDING
This research was supported by the National Institutes of Health R15 NS061309-01 (KME).

CONFLICT OF INTEREST
There are no conflicts of interest to be disclosed by any of the authors.

REFERENCES
Anderson JG, Cooney PT, Erikson KM. Inhibition of DAT function attenuates manganese accumulation in the globus pallidus. Environ Toxicol Pharmacol 2007;23:179–84.

Anderson JG, Fordahl SC, Cooney PT, Weaver TL, Colyer CL, Erikson KM. Manganese exposure alters extracellular GABA, GABA receptor and transporter protein and mRNA levels in the developing rat brain. NeuroTox 2008;29:1044–53.

Baquer NZ, Nothersall JS, Greenbaum AL, McLean P. The modifying effect of manganese on the enzymic profiles and pathways of carbohydrate metabolism in rat liver and adipose tissue during development. Biochem Biophys Res Commun 1974;62(3): 634–41.

Bouchard MF, Laforest F, Vandelac L, Bellinger D, Mergler D. Hair manganese and hyperactive behaviors: pilot study of school-age children exposed through tap water. EHP 2007;115(1):122–7.

BouchardMF, Sauve S, Barbeau B, Legrand M, BrodeurM, Bouffard T, Limoges E, Bellinger DC, Mergler D. Intellectual impairment in school-age children exposed tomanganese from drinking water. EHP 2011;119(1):138–43.

Brock AA, Chapman SA, Ulman EA, Wu G. Dietary manganese deficiency decreases rat hepatic arginase activity. J Nutr 1994;124(3):340–4.

Cai T, Che H, Yao T, Chen Y, Huang C, Zhang W, Du K, Zhang J, Cao Y, Chen J, Luo W. Manganese induces tau hyperphosphorylation through the activation of ERK MAPK pathway in PC12 cells. Toxicol Sci 2011;119(1):169–77.

Calabresi P, Ammassari-Teule M, Gubellin P, Sancesario G, Morello M, Centonze D,Marfia GA, Saulle E, Passino E, Picconi B, Bernardi G. A synaptic mechanism underlying the behavioral abnormalities induced by manganese intoxication. Neurobiol Dis 2001;8: 419–32.

Castaneda TR, de Prado BM, Prieto D, Francisco M. Circadian rhythms of dopamine, glutamate and GABA in the striatum and nucleus accumbens of the awake rat: modulation by light. J Pineal Res 2004:177–85.

CersosimoMG, KollerWC. The diagnosis ofmanganese-induced parkinsonism. NeuroTox 2006;27:340–6.

Chua AC, Morgan EH. Effects of iron deficiency and iron overload on manganese uptake and deposition in the brain and other organs of the rat. Biol Trace Elem Res 1996;55(1–2):39–54.

Chun HS, Lee H, Son JH. Manganese induces endoplasmic reticulum (ER) stress and activates multiple caspases in nigral dopaminergic neuronal cells, SN4741. Neurosci Lett 2001;316:5–8.

Cowan DM, Zheng W, Zou Y, Shi X, Chen J, Rosenthal FS, Fan Q. Manganese exposure among smelting workers: relationship between blood manganese–iron ratio and early onset neurobehavioral alterations. NeuroTox 2009;30(6):1214–22.

Crossgrove J, Zheng W. Manganese toxicity upon overexposure. NMR Biomed 2004;17: 544–53.

Davis CD, Greger JL. Longitudinal changes of manganese-dependent superoxide dismutase and other indexes of manganese and iron status in women. Am J Clin Nutr 1992;55(3):747–52.

deHaas R,NijdamA,Westra TA, KasMJH,Westenberg HGM. Behavioral pattern analysis and dopamine release in quinpirole-induced repetitive behavior in rats. J Psychopharmacol 2010:1–8.

Demougeot C, Garnier Pl, Mossiat C, Bertrand N, Giroud M, Beley A, Marie C. N-Acetylaspartate, a marker of both cellular dysfunction and neuronal loss: its relevance to studies of acute brain injury. J Neurochem 2001;77(2):408–15.

Dorman CD, Struve MF, Wong AW, Dye JA, Robertson ID. Correlation of brain magnetic resonance imaging changes with pallidal manganese concentrations in rhesus monkeys following subchronic manganese inhalation. Toxicol Sci 2006;92(1): 219–27.

Dorman CD, Struve MF, Norris A, Higgings AJ. Metabolomic analyses of body fluids after subchronic manganese inhalation in rhesus monkeys. Toxicol Sci 2008;106(1): 46–54.

Erikson KM, Syversen T, Steinnes E, Aschner M. Globus pallidus: a target region for divalent metal accumulation associated with dietary iron deficiency. J Nutr Biochem 2004;15:335–41.

Erikson KM, Dorman DC, Lash LH, Aschner M. Manganese inhalation by rhesus monkeys is associated with brain regional changes in biomarkers of neurotoxicity. Toxicol Sci 2007;97(2):459–66.

Farias AC, Cunha A, Benko CR, McCracken JT, Costa MT, Farias LG, Cordeiro ML. Manganese in children with attention-deficit/hyperactivity disorder: relationship with methylphenidate exposure. J Child Adolesc Psychopharmacol 2010;20(2):113–8.

Fitsanakis VA, Au C, Erikson KM, Aschner M. The effects of manganese on glutamate, dopamine and γ-aminobutyric acid regulation. Neurochem Int 2006;48:426–33.

Fitsanakis VA, Zhang N, Anderson JG, Erikson KM, Avison MJ, Gore JC, Aschner M. Measuring brain manganese and iron accumulation in rats following 14 weeks of low-dose manganese treatment using atomic absorption spectroscopy and magnetic resonance imaging. Toxicol Sci 2008;103(1):116–24.

Flagel SB, Robinson TE. Quantifying the psychomotor activating effects of cocaine in the rat. Behav Pharmacol 2007;18:297–302.

Fordahl SC, Anderson JG, Cooney PT, Weaver TL, Colyer CL, Erikson KM. Manganese exposure inhibits the clearance of extracellular GABA and influences taurine homeostasis in the striatum of developing rats. NeuroTox 2010;31:639–46.

Garcia SJ, Gellein K, Syversen T, Aschner M. A manganese-enhanced diet alters brain metals and transporters in the developing rat. Toxicol Sci 2006;92(2):516–25.

Gianutsos G, Murray MT. Alterations in brain dopamine and GABA following inorganic or organic manganese administration. NeuroTox 1982;3:75–81.

Guilarte TR, McGlothan JL, Degaonkar M, Chen MK, Barker PB, Syversen T, Schneider JS. Evidence for cortical dysfunction and widespread manganese accumulation in the nonhuman primate brain following chronic manganese exposure: a 1H-MRS and MRI study. Toxicol Sci 2006;94(2):351–8.

Halket JM, Waterman D, Przyborowska AM, Patel RKP, Fraser PD, Bramley PM. Chemical derivatization and mass spectral libraries in metabolic profiling by GC/MS and LC/MS/MS. J Exp Bot 2005;56(410):219–43.

Harkness JE, Wagner JE. The biology and medicine of rabbits and rodents. 3rd edition. Philadelphia: Lea and Febiger; 1989.

HMDB. Human metabolome database web site. http://www.hmdb.ca/2011. Accessed: January 18, 2011.

Hurley LS, Keen CL. Trace elements in human and animal nutrition. In: Mertz W, editor. 5th ed. San Diego, CA: Academic Press; 1987. p. 185–223.. vol. 1.

Kawamura R, Ikuta H, Fukuzumi S, Yamada R, Tsubaki S. Intoxication by manganese in well water. Kitasato Arch Exp Med 1941;18:145–71.

Kern CH, Stanwood GD, Smith DR. Preweaning manganese exposure causes hyperactivity, disinhibition, and spatial learning and memory deficits associated with altered dopamine receptor and transporter levels. Synapse 2010;64:363–78.

Kim Y, Kim JW, Ito K, Hisanaga N, Cheong HK, Kim KS, Moon Y. Positron emission tomography (PET) in differentiating manganism from idiopathic Parkinsonism. J Occup Health 1999;41:91–4.

Kim YS, Maruvada P, Milner JA. Metabolimics in biomarker discovery: future uses for cancer prevention. Future Oncol 2008;4(1):93-102.

NTP. Toxicology and carcinogenesis studies of manganese (II) sulfate monohydrate in F344/N rats and B6C3F1 mice (feed study). National toxicology program. Technical report series 428. RISKLINE 94030007; 1993.

O'Donoghue JL. Clinical neurologic indices of toxicity in animals. Environ Health Perspect 1996;104(Suppl. 2):323–30.

Oresic M, Vidal-Puig A, Hanninen V. Metabolomic approaches to phenotype characterization and applications to complex diseases. Expert Rev Mol Diagn 2006;6(4): 575–85.

Pal PK, Samii A, Calne DB.Manganese neurotoxicity: a reviewof clinical features, imaging and pathology. NeuroTox 1999;20:227–38.

Pan L, Qiu Y, Chen T, Lin J, Chi Y, Su M, Zhao A, Jia W. An optimized procedure for metabonomic analysis of rat liver tissue using gas chromatography/time-of-flight mass spectrometry. J Pharm Biomed Anal 2010;52(4):589–96.

Patil S, Melrose J, Chan C. Involvement of astroglial ceramide in palmitic acid-induced Alzheimer-like changes in primary neurons. Eur J Neurosci 2007;26:2131–41.

Patil S, Balu D, Melrose J, Chan C. Brain region-specificity of palmitic acid-induced abnormalities associated with Alzheimer's disease. BMC Res Notes 2008;1:20.

Perl DP, Olanow CW. The neuropathology of manganese-induced Parkinsonism. J Neuropathol Exp Neurol 2007;66(8):675–82.

Pradat PF, Dib M. Biomarkers in amyotrophic lateral sclerosis: facts and future horizons. Mol Diagn Ther 2009;13(2):115–25.

Qiu Y, Cai G, Su M, Chen T, Zheng X, Xu Y, Ni Y, Zhao A, Xu LX, Cai S, Jia W. Serum metabolite profiling of human colorectal cancer using GC–TOFMS and UPLC–QTOFMS. J Proteome Res 2009;8(10):4844–50.

Reghunandanan V, Reghunandanan R. Neurotransmitters of the suprachiasmatic nuclei. J Circadian Rhythm 2006;4(2):1-20.

Ronchetti IP, Contri MB. Elastic fiber during development and aging. Microsc Res Tech 1997;38:428–35.

Scheer FA, Kalsbeek A, Buijs RM. Cardiovascular control by the suprachiasmatic nucleus: neural and neuroendocrine mechanisms in human and rat. Biol Chem 2003;384: 697–709.

Schneider JS, Decamp E, Koser AJ, Fritz S, Gonczi H, Syversen T, Guilarte TR. Effects of chronic manganese exposure on cognitive and motor functioning in non-human primates. Brain Res 2006;1118(1):222–31.

Scorpio RM, Masoro EJ. Differences between manganese and magnesium ions with regard to fatty acid biosynthesis, acetyl-coenzyme a carboxylase activity and malonyl-coenzyme A decarboxylation. Biochem J 1970;118:391–9.

Shobab LA, Hsiung GYR, Feldman HH. Cholesterol in Alzheimer's disease. Lancet Neurol 2005;4:841–52.

Steele AD, Jackson WS, King OD, Lindquist S. The power of automated high-resolution behavior analysis revealed by its application to mouse models of Huntington's and prion diseases. PNAS 2007;104:1983–8.

Suzuki K, Miyamoto M, Miyamoto T, Iwanami M, Hirata K. Sleep disturbances associated with Parkinson's disease. Park Dis 2011;2011(219056):1-10.

Tjalkens RB, Zoran MJ, Mohl B, Barhoumi R. Manganese suppresses ATP-dependent intercellular calcium waves in astrocyte networks through alteration of mitochondrial and endoplasmic reticulum calcium dynamics. Brain Res 2006;1113:210–9.

Vacher CM, Gassmann M, Desrayaud S, Challet E, Bradaia A, Hoyer D, Waldmeier P, Kaupmann K, Pévet P, Bettler B. Hyperdopaminergia and altered locomotor activity in GABAB1-deficient mice. J Neurochem 2006;97:979–91.

Wagner S, Sagiv N, Yarom Y. GABA-induced current and circadian regulation of chloride in neurones of the rat suprachiasmatic nucleus. J Physiol 2001;537(3):853–69.

Wasserman GA, Liu X, Parvez F, Ahsan H, Levy D, Factor-Litvak P, Kline J, van Geen A, Slavkovich V, Lolacono NJ, Cheng Z, Zheng Y, Graziano JH. Water manganese exposure and children's intellectual function in Araihazar, Bangladesh. Environ Health Perspect 2006;114:124–9.

Witholt R, Gwiazda RH, Smith DR. The neurobehavioral effects of subchronic manganese exposure in the presence and absence of pre-parkinsonism. Neurotoxicol Teratol 2000;22:851–61.

Youdim MB, Yehuda S. Iron deficiency induces reversal of dopamine dependent circadian cycles: differential resonse to D-amphatamine and TRH. Peptides 1985;6:851–5.

Youdim MB, Green AR, Bloomfield MR, Mitchell BD, Heal DJ, Grahame-Smith DG. The effects of iron deficiency on brain biogenic monoamine biochemistry and function in rats. Neuropharmacology 1980;19:259–67.